Characterization of the Iron Phase in CNx−Based Oxygen Reduction Reaction Catalysts

ARTICLE *in* THE JOURNAL OF PHYSICAL CHEMISTRY C · JANUARY 2007

Impact Factor: 4.77 · DOI: 10.1021/jp0651236

Characterization of the Iron Phase in CN_x-Based Oxygen Reduction Reaction Catalysts

Paul H. Matter,[†] Eugenia Wang,[†] Jean-Marc M. Millet,[‡] and Umit S. Ozkan*[,†]

Department of Chemical Engineering, The Ohio State University, 140 W. 19th Avenue, Columbus, Ohio, and Institut de Recherches sur la Catalyse, CNRS, 2 avenue Albert Einstein, 69626 Villeurbanne Cedex, France

Received: August 9, 2006; In Final Form: November 2, 2006

Catalysts for the oxygen reduction reaction were prepared from the pyrolysis of acetonitrile at 900 °C over iron particles on various supports. The iron phases present in the active materials were characterized by XRD, TEM, and Mössbauer spectroscopy. Typically, the iron particles were encased in carbon after pyrolysis, explaining how they could survive subsequent acid washes. The Fe phases present included metallic gamma iron, cementite, and two oxidized phases. Although the relative abundance of the phases varied with different supports, with treatment time, and after washing, there was no apparent correlation between the presence or abundance of a phase and activity. The phases present are consistent with Fe particles used to catalyze the formation of carbon fibers by catalytic chemical vapor deposition. After being washed with acid, there was no evidence for the presence of nitrogen-stabilized Fe sites on the carbon surface. These results support the hypothesis that Fe catalyzes the formation of ORR-active carbon nanostructures during pyrolysis at 900 °C in a carbon and nitrogen atmosphere and is not part of an active site itself.

Introduction

The low availability of platinum currently hinders the large-scale commercialization of proton exchange membrane (PEM) fuel cells because of the platinum requirements of PEM fuel cell cathodes. Developing alternative oxygen reduction reaction (ORR) catalysts is therefore a high priority among fuel cell research topics. Alternative catalysts formed from heat-treated iron, nitrogen, and carbon compounds have shown promising results as potential replacements for platinum.[1] Although these alternative catalysts operate with activities that are comparable to that of platinum (within a 100 mV potential drop or $^1/_{10}$ times the kinetic current at constant voltage), further improvements in activity would be desirable to improve cell efficiency and power density.[1]

Obtaining a better understanding of the nature of the active site in heat-treated Fe/N/C materials could potentially lead to the development of more active catalysts for the ORR. Initially, this class of heat-treated catalysts was derived from pyrolyzed organic macrocycles such as Fe porphyrins or phthalocyanines.[2−4] Work has shown that up to 700 °C metal center active sites can still remain in the materials.[2] Bouwkamp-Wijnoltz et al. conducted cyclic voltammetry experiments with in situ Mössbauer spectroscopy.[5] The work demonstrated that metal centers operating through a redox mechanism likely remain in macrocycles treated up to 700 °C. However, pyrolyzed transition-metal macrocycles maintain activity at even higher treatment temperatures, at which point the macrocycles decompose and metal particles form.[6−12] Moreover, active catalysts can be prepared from the pyrolysis of metal particles in the presence of a non-macrocyclic nitrogen and carbon source.[13−16] Some researchers believe that metal ions stabilized by nitrogen surface groups (that can form either during treatment or after exposure of the sample to the acid electrolyte) are the source of ORR activity. Several studies using secondary ion mass spectroscopy,[16,17] Mössbauer spectroscopy,[18] and theoretical calculations[19] support this hypothesis. Contrastingly, some researchers have proposed that metal particles (such as Fe or Co) merely catalyze the formation of an active site comprising nitrogen-doped carbon surface groups.[20−22] Supporting this hypothesis is the fact that nitrogen-doped carbon experimentally[23,24] and theoretically[25,26] has shown elevated activity for the ORR compared to carbon. Furthermore, conductive polymers that contain nitrogen groups display ORR activity.[27]

Recent research in our group has shown that one possible explanation for the role of Fe and Co in heat-treated nitrogen-doped carbon ORR catalysts is as a catalyst for the formation of nanostructures with increased edge plane exposure.[14,23,24,28,29] Carbon edge planes are known to be more active in electrochemical reactions,[30−32] and most proposed active sites would be found on the edge of a carbon plane or within defects of the plane. Because the most active catalysts always contained Fe or Co, our group's previous work did not convincingly demonstrate that a metal-based active site no longer remains.[14,23,24,29] However, it should be mentioned that highly active catalysts could be prepared from acetonitrile decomposition over high-purity alumina (less than 1 ppm metal contamination), demonstrating that the metal sites are not required for elevated activity compared to carbon.[23,24]

In the current study, the phase of iron in active ORR catalysts prepared from acetonitrile pyrolysis over various supports is investigated. In every case, iron particles catalyzed the formation of carbon fibers with significant edge plane exposure. The role of Fe as a catalyst for nitrogen-doped carbon structures with edge plane exposure rather than as part of an active ORR site is considered while characterizing the Fe phases with XRD, TEM, and Mössbauer spectroscopy.

Experimental Methods

Catalyst Preparation. Nitrogen-doped carbon nanofibers were prepared from the chemical vapor deposition of acetonitrile

* Corresponding author. E-mail: ozkan.1@osu.edu.
[†] The Ohio State University.
[‡] CNRS.

10.1021/jp0651236 CCC: $37.00
Published on Web 01/03/2007

over supported iron particles. As reported elsewhere, vulcan carbon (VC),[14] alumina,[23,24] silica,[28,29] and magnesia[28,29] were examined as supports for iron. Each support was impregnated with 2 wt % Fe in the form of an acetate salt. Next, acetonitrile decomposition, or pyrolysis, was carried out by adding 2.0 g of the powder support to a quartz calcination boat and sealing it inside a quartz tube furnace. The temperature was then ramped at 10 °C/min up to the treatment temperature under the carrier gas (N_2 unless noted otherwise) flowing at 150 sccm. Once the furnace reached 900 °C, the room-temperature carrier gas was saturated with acetonitrile ($P_{vap} = 72.8$ mmHg) using a bubbler before being sent to the furnace. After the treatment was complete (times varied), samples were cooled to room temperature under the carrier gas. Carbon deposited on the alumina sample could be purified by washing with HF acid, whereas carbon deposited on the silica or magnesia support could be purified with KOH or HCl, respectively.

To carry out sample analysis with Mössbauer spectroscopy, ^{57}Fe-enriched samples were also prepared. First, ^{57}Fe metal (Cambridge Isotope Labs, Inc.) was dissolved in glacial acetic acid. The enriched solution was then diluted with an Fe acetate salt solution such that the final impregnated precursor would contain 0.08 wt % ^{57}Fe and 2 wt % Fe overall. The precursors were treated under the same conditions described in the previous paragraph. It should be noted that the ^{57}Fe-enriched samples lost a large amount of mass during the temperature ramp (around 40%) presumably from the loss of acetic acid (used to dissolve ^{57}Fe) in the sample. The distinct smell of acetic acid was apparent in this precursor prior to the treatments.

TEM. Transmission electron microscopy was performed with a Philips CM300 Ultra-Twin FEG TEM and also a Philips Tecnai TF20. Samples were supported by lacey-formvar/carbon, which was supported by a 200 mesh copper grid. The samples were dispersed with excess ethanol before being deposited on the grid.

X-ray Diffraction. X-ray diffraction patterns were obtained with a Bruker D8 diffractometer using Cu K_α radiation. Samples were supported by polyethylene holders with a 0.5-mm-deep reservoir for the powder samples. Patterns were recorded between 10 and 90° 2Θ.

Mössbauer Spectroscopy. Mössbauer spectroscopy was conducted using ^{57}Co/Rh as the γ-ray source and a conventional constant acceleration Mössbauer spectrometer. The isomer shifts are given with respect to α-Fe. All of the samples were exposed to the ambient atmosphere, and the spectra were taken at room temperature. The areas of the observed signals have been used to evaluate the relative populations of the different iron species, assuming an equal free recoil fraction for all species.

Activity and Conductivity Testing. ORR activity testing has been described in more detail elsewhere.[14] Briefly, the sample activity for the ORR was gauged in a PAR model RDE0018 half-cell setup using 0.5 M H_2SO_4 as the electrolyte, a Ag/AgCl reference electrode, and a platinum wire counter electrode. Cyclic voltammetry experiments were conducted in the solution sparged with argon to obtain a background current and then sparged in oxygen to measure the ORR current. The details of these experiments were described previously.[14] Activities were compared on the basis of potential drops from theory required for oxygen reduction.

Results and Discussion

Activity Testing Results. All of the samples prepared displayed high activity for the ORR, as reported elsewhere for the vulcan carbon (VC)-,[14] alumina-,[23] silica-,[29] and magnesia[29]-supported samples. The CN_x prepared from 2 wt % Fe/Al_2O_3 treated with acetonitrile at 900 °C for 2 h and washed with HF acid had the highest ORR activity of the group, within 100 mV of the activity of a commercial 20 wt % Pt/VC catalyst. The catalyst prepared on vulcan carbon had lower activity than the other samples (200 mV less than Pt); however, the vulcan carbon support could not be purified from the active fibers by acid leaching. In both cases, preparing the catalyst with ^{57}Fe did not affect the activity within a ±30 mV potential drop difference.

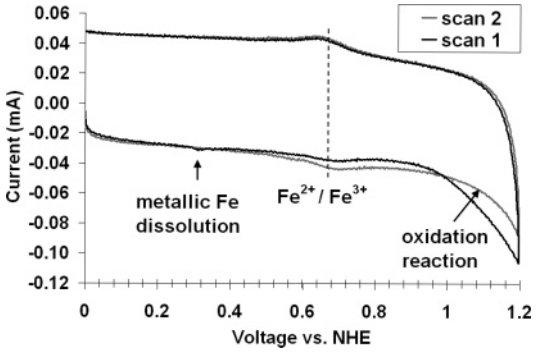

Figure 1. Initial cyclic voltammetry experiments (before CVs are repeatable) for CN_x−Fe/VC in argon-sparged 0.5 M H_2SO_4.

It should be mentioned that during electrochemical testing, dissolution of Fe and possibly a subsequent Fe^{3+}/Fe^{2+} redox reaction was apparent in the CN_x−Fe/VC samples during initial CVs in argon. Figure 1 shows some representative results. The scans sweep from 1.2 to 0.0 to 1.2 V versus NHE at a rate of 50 mV/s, and typically took about five scans until the current was repeatable. The metallic iron dissolution was much more pronounced if higher Fe loadings were used (data not shown). This dissolution has been reported by other researchers studying pyrolyzed Fe/N/C materials.[33,34] A possible redox reaction was also observed after the Fe dissolution. This reaction occurs at the potential expected for the Fe^{3+}/Fe^{2+} redox reaction in sulfuric acid.[35] In contrast, for the alumina-, silica-, and magnesia-supported samples, which were all washed with an acid prior to electrochemical testing, no such reactions in the electrolyte were apparent (data not shown). In one instance, unwashed CN_x−Fe/Al_2O_3 was tested, and the same dissolution peak and redox peaks were apparent. Interestingly, in all cases an additional oxidation reaction was apparent for the samples during the initial CVs at higher potentials. It is believed that oxidation of the carbon surface may be occurring; however, further work is required to confirm this hypothesis.

XRD. The full XRD patterns for the vulcan carbon,[14] alumina,[23] silica,[28] and magnesia[28] samples were previously reported. In the region between 40 and 54° 2Θ, shown in Figure 2, peaks from several metallic species and from graphite can be found. Identification of the peaks with only XRD is difficult because of the low Fe content in the samples. On the basis of the weight change that occurred during acetonitrile decomposition, the Fe content of CN_x−Fe/VC is 1.4%. On the basis of TPO/TGA of washed samples and XPS analysis of the post-TPO ash, the Fe content of the other samples is approximately 1.5−4%. However, it is apparent that a mixture of metallic and carbide species could be present, as was reported by Faubert et al. for carbon-supported Fe particles treated in acetonitrile vapors.[36] Although a clear picture of what Fe phases are present cannot be obtained from XRD, the patterns indicate that a small amount of some crystalline Fe phases is present, even after the acid washes. For comparison, the pattern for CN_x grown from Co/MgO by the same procedure is shown. The peaks for metallic Co were very prevalent in this sample.

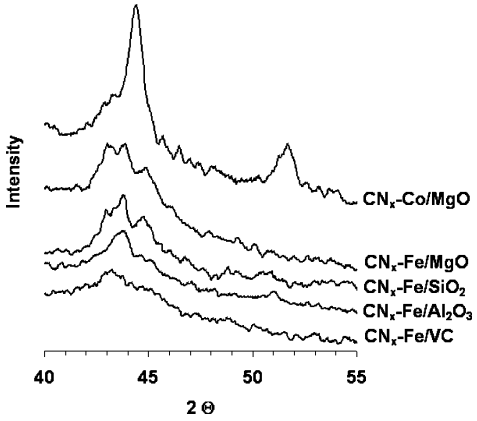

Figure 2. XRD patterns showing the region rich in peaks from metal species for various catalysts.

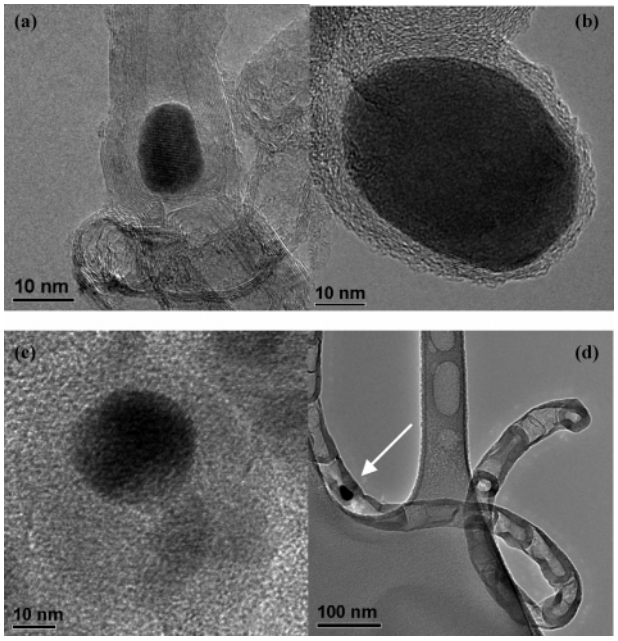

Figure 3. TEM images showing the various locations of metal particles in (a) CN_x-Fe/Al_2O_3, (b and c) CN_x-Fe/VC, and (d) CN_x-Fe/MgO.

TEM. Electron microscopy imaging shows how metal particles can survive the acid-leaching steps. Iron particles within the sample were observed to be encased by several layers of graphitic carbon (Figure 3). The metal particles could be found at the ends of nanotubes, within compartmentalized fibers, or by themselves encased in graphite. From imaging, some long-range order in the metal particles was apparent. Other researchers have used electron diffraction to characterize metal particles that have catalyzed the formation of carbon nanotubes.[37] These researchers have reported metallic and several carbide phases within metal particles. However, electron diffraction was not conducted here; instead, bulk Fe phase characterization was done using Mössbauer spectroscopy. No metal could be detected from XPS analysis of washed samples, likely because the metal was covered by several layers of carbon and the metal compositions are low.

Mössbauer Spectroscopy. The Mössbauer spectrum for the unwashed CN_x-Fe/Al_2O_3 is shown in Figure 4. Using the guidelines outlined in Table 1 as a basis for initial parameter guesses, the spectrum fits nicely to four different species corresponding to a single-line subspectrum, a sextet, and two doublets. The sextet with an internal magnetic field of ~210 kOe can be assigned unambiguously to cementite, Fe_3C.[37−39]

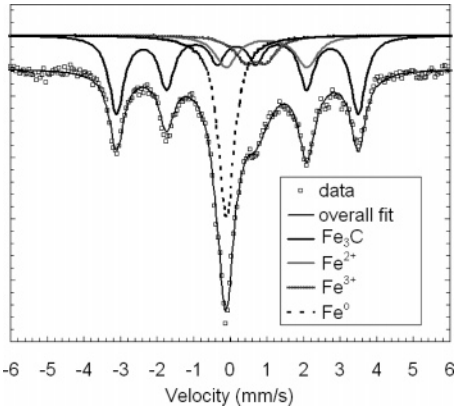

Figure 4. Mössbauer spectrum for 2 wt % Fe/Al_2O_3 treated for 2 h at 900 °C with acetonitrile. (The sample was not washed.) Subspectra are derived from a least-squares fit.

The single line corresponds either to γ-Fe or to superparamagnetic α-Fe. Both attributions are difficult to sustain (or explain). At the reaction temperature, the γ-Fe phase should be the stable phase formed, but it should be converted to α-Fe, which is the stable phase when brought back to room temperature. However, small superparamagnetic α-Fe particles are very difficult to observe because they readily oxidize when they come into contact with any oxidant.[40] In our case, both hypotheses could be explained by the fact that the particles corresponding to metallic iron are encased in the carbon fibers. For γ-Fe, the encasement should prevent the phase transition from occurring because it does not allow the corresponding cell volume expansion. For α-Fe, it would prevent the oxidation of the nanoparticles. The fact that they are not dissolved even after washing with HF supports both assertions. To determine which hypothesis was right, we conducted via Mössbauer spectroscopy an analysis of a sample containing the single line in its room-temperature spectrum at 77 K. The fit of the spectrum was similar to that recorded at room temperature, as will be discussed. Such a result leads us to consider that the single lines correspond to a pure paramagnetic species (i.e., γ-Fe). The two doublets correspond to ferric and ferrous species, but it is not possible to make definitive assignments as to the exact nature of the species. Most likely, the Fe^{3+} forms through the oxidation of partially exposed metallic particles, with the Fe^{2+} being an intermediate.

Table 2 reports the parameters for all of the fits that will be discussed. The Fe phases present may reveal some information about the mechanism of fiber growth in the samples. All of the samples contained a significant amount of metallic Fe (γ-Fe). Baker et al. observed metallic Fe, with an assignment to γ-Fe, in samples where fibers grew from graphite-supported Fe.[41] The determined mechanism for fiber growth in these materials began with Fe spreading on the support surface, followed by the adsorption of carbon, and then elemental carbon growth from the Fe, while the Fe remained on the surface. Cementite (Fe_3C) is another species observed in the acetonitrile heat-treated materials, although its abundance varies between samples. Cementite has been observed by Audier et al.[37] and Herreyre et al.[38] in materials where carbon fibers also grew from Fe particles. The mechanism in this case involved the adsorption of carbon onto the metal, the diffusion of carbon through the particle, and the deposition of carbon out of the other end, resulting in the metal being lifted off of the support surface during fiber growth.[42] The ferric and ferrous species may correspond to oxide or oxi-carbide (FeO_x, FeO_xC_y) formed when heating the supported acetate under acetonitrile. They may also

TABLE 1: Parameter Ranges for Mössbauer Spectra of Common Fe Species Used as a Basis for Initial Guesses for the Parameter Fits

phase	splitting	isomer shift δ (mm/s)	quadropole splitting Δ (mm/s)	H (kOe)	ref
α-Fe (large particles)	sextet	~0	~0	330	37, 38
α-Fe (small particles) or γ-Fe	singlet	~0	~0	0	38
cementite, Fe_3C	sextet	0.18−0.25	0.01−0.9	200	37−39
α-Fe_2O_3 (large particles)	sextet	0.35−0.37	1.00−1.02	550	38
α-Fe_2O_3 (small particles)	doublet	0.35−0.37	1.00−1.02	0	38
high-spin Fe^{3+} species	doublet	0.2−0.7	0.0−1.3	0	49, 50
high-spin Fe $^{2+}$ species	doublet	0.9−1.9	1.0−2.5	0	49, 50

TABLE 2: Mössbauer Parameters Calculated from the Specta of the Compounds Recorded at 25 °C (unless Otherwise Noted)[a]

sample	species	rel. int. (%)	δ (mm/s)	Δ (mm/s)	H (kOe)
Fe/Al_2O_3 - 2 h	Fe_3C	46	0.20	0.00	204
	Fe^0	30	−0.09	0.00	0
	Fe^{2+}	14	1.01	2.19	0
	Fe^{3+}	10	0.70	0.57	0
Fe/Al_2O_3 - 2 h	Fe_3C	38	0.18	0.00	204
(HF washed)	Fe^0	49	−0.10	0.00	0
	Fe^{2+}	4	1.00	2.18	0
	Fe^{3+}	9	0.55	0.50	0
Fe/Al_2O_3 - 2 h	Fe_3C	38	0.29	0.00	242
(HF washed)	Fe^0	51	−0.01	0.00	0
Recorded at 77 K	Fe^{2+}	1	1.18	2.18	0
	Fe^{3+}	10	0.66	0.58	0
Fe/Al_2O_3 - 20 min	Fe_3C	39	0.20	0.00	201
	Fe^0	31	−0.09	0.00	0
	Fe^{2+}	8	1.06	1.96	0
	Fe^{3+}	22	0.61	0.53	0
Fe/Al_2O_3 - 12 h	Fe_3C	55	0.18	0.00	202
	Fe^0	17	−0.09	0.00	0
	Fe^{2+}	21	1.04	2.19	0
	Fe^{3+}	7	0.69	0.55	0
	Fe_3C	29	0.20	0.00	205
Fe/VC - 2 h	Fe^0	53	−0.07	0.00	0
	Fe^{2+}	12	1.01	2.19	0
	Fe^{3+}	6	0.63	0.58	0
Fe/SiO_2 - 2 h	Fe_3C	42	0.22	0.00	209
(KOH and HCl washed)	Fe^0	29	−0.05	0.00	0
	Fe^0	14	0.05	0.00	332
	Fe^{2+}	9	1.03	1.34	0
	Fe^{3+}	6	0.30	0.89	0
Fe/MgO - 2 h	Fe_3C	53	0.18	0.00	206
(HCl washed)	Fe^0	27	−0.09	0.00	0
	Fe^0	8	−0.04	0.00	332
	Fe^{2+}	5	1.09	1.93	0
	Fe^{3+}	7	0.34	0.50	0

[a] δ, isomer shift (given with respect to α Fe); Δ, quadrupolar splitting; and H, internal magnetic field.

be formed after reaction from small metallic particles not completely encased in the carbon fibers when the solid is handled under ambient air. Because there is evidence of a carbide species and both nitrogen and carbon were present in the fibers, one may also expect a nitride species to be formed upon treatment with acetonitrile. However, the literature of Mössbauer spectra for various forms of iron nitride does not report any spectra with similar parameters.[43−48]

The Mössbauer spectra contained the same four species regardless of treatment time, although the relative intensities of the species changed. It should be pointed out that the initial guess used for these samples was based on the initial fit for the sample treated for 2 h. The spectra in Figure 5a clearly shows the change in the relative intensities of the sextet yielding carbide species for treatments of 20 min, 2 h, and 12 h. From the Figure, it can be seen that the carbide contribution grows with treatment time while the metallic Fe phase decreases. The change in the relative contributions of all of the species with time is also illustrated in Figure 5b. The same effect was observed with Mössbauer spectroscopy for Fe-based CO disproportionation catalysts treated for various times in a carbon-rich atmosphere.[38] The oxidized Fe phases as a whole remain relatively constant, although the Fe^{3+} decreases and the Fe^{2+} increases with time. There are three possible explanations for this. First, the Fe^{2+} may be formed by reduction under acetonitrile of the ferric species initially formed. A second possibility is that the Fe^{2+} and Fe^{3+} species result from the oxidation of small Fe particles in air when the sample was exposed to atmospheric conditions several weeks before being analyzed. A third possibility is that the Fe^{2+} is a nitride or oxi-nitride phase forming in a similar manner to the carbide phase and thus increasing for the same reason that the carbide phase increases. It should be pointed out that we have yet to find a nitride phase reported in the literature that has an isomer shift and quadrapole splitting that are similar to those of the observed Fe^{2+} phase.

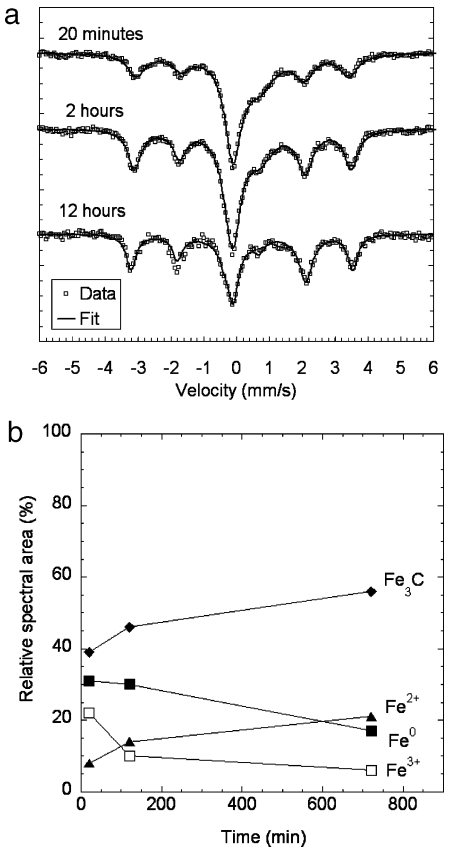

Figure 5. Evolution of the Mössbauer spectra with treatment time for 2 wt % Fe/Al_2O_3: (a) spectra and overall fits and (b) changes in the relative content of Fe species.

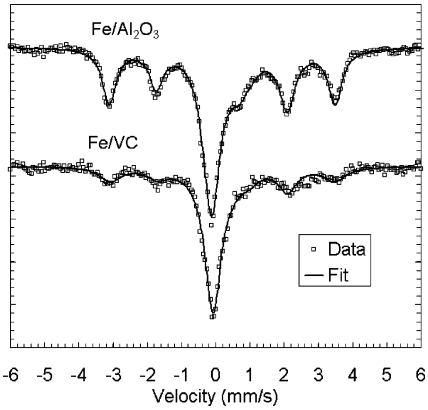

Figure 6. Comparison of Mössbauer spectra for VC and alumina-supported Fe samples treated for 2 h at 900 °C with acetonitrile. Solid lines are derived from a least-squares fit.

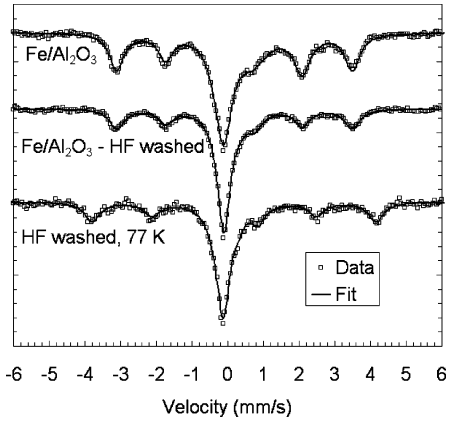

Figure 7. Comparison of Mössbauer spectra for HF-washed and unwashed alumina-supported Fe samples treated for 2 h at 900 °C with acetonitrile. A spectrum of the washed sample recorded at 77 K is also shown for comparison. Solid lines are derived from a least-squares fit.

Interestingly, when the Fe was supported by carbon rather than alumina, the spectra contained the same four species but had significantly different contributions from these species. A comparison of the spectra is shown in Figure 6. When Fe is supported by vulcan carbon, it appears that Fe carbide is less likely to form and metallic Fe is preferred. The Fe^{2+} is only slightly larger in the sample with more carbide, so little can be said of its nature on the basis of these results.

The Mössbauer spectra also changed after the alumina-supported sample was washed with HF acid. The spectra after HF washing is shown in Figure 7. Again, the same species could be fit to the deconvolution; however, the ratio of the species changed. Specifically, the oxidized phases and the carbide phase decreased after the wash. Apparently, the carbide phase is not protected as well as the metallic phase. It should be noted that when these oxidized species contribute such a small amount to the spectra, deconvolution becomes difficult, especially with the noise present in the signal. The relative compositions for the samples are shown in Table 2 for comparison. The washed sample was analyzed a second time at 77 K instead of room temperature. The fact that the singlet remained was the basis for its assignment to paramagnetic γ-Fe. Changes in the isomer shifts and magnetic field of the other species are expected at lower temperatures. The drop in the contribution of the Fe^{2+} species may be due to the fact that this analysis was performed several months after the original analysis, particularly if Fe^{2+} is an intermediate for metallic iron being oxidized to Fe^{3+}.

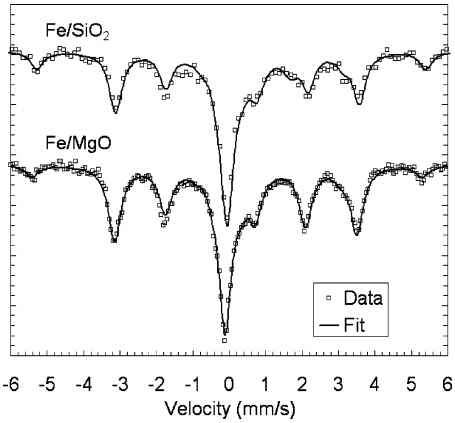

Figure 8. Comparison of Mössbauer spectra for magnesia- and silica-supported Fe samples treated for 2 h at 900 °C with acetonitrile and subsequently washed. Solid lines are derived from a least-squares fit.

Highly active catalysts could also be prepared from acetonitrile pyrolysis over Fe supported by silica or magnesia, rather than alumina.[29] In the case of silica, the carbon can be purified from the support by washing with 1 M KOH, and in the case of magnesia, the carbon can be purified using 1 M HCl. The spectra of CN_x−Fe/SiO_2 and CN_x−Fe/MgO are shown in Figure 8. The velocity range for recording the CN_x−Fe/SiO_2 spectra was larger than the one used for the spectra presented in previous Figures, which is why the number of points for the same range in the raw data appears to be smaller. In the case of these samples, an additional sextet corresponding to α-Fe was present. Previously, both of these samples were reported to contain a mixture of large and small fibers, and TEM imaging revealed some large Fe particles present in the samples.[28] Thus, the presence of both small and large α-Fe particles in these samples could explain the super paramagnetic and ferromagnetic behavior, respectively. The washed Fe/Al_2O_3 sample contains only small fibers and Fe particles and likewise does not have the additional α-Fe sextet. All of the samples also contain some oxidized Fe. Interestingly, the parameters for the oxidized phase seem to be affected during the wash and vary depending on the leaching agent used.

On the basis of these results, there is no correlation between an Fe phase and ORR activity. The activity increased after the acid wash (by 60 mV), so ORR activity cannot be readily attributed to the carbide or oxidized Fe phases, considering that the content of these species decreased after the wash. Additionally, the metallic Fe phase preferentially formed in the VC-supported sample but had lower activity, so metallic Fe cannot be assigned as the source of activity because this sample was less active. It must be pointed out that the Fe contents of the samples are similar: 1.4, 1.6, and ~1.4 wt % for the CN_x−Fe/VC, CN_x−Fe/Al_2O_3 (unwashed), and CN_x−Fe/Al_2O_3 (HF washed) samples, respectively. Previously, we hypothesized that Fe merely acts as the catalyst for the formation of an active site by catalyzing the growth of carbon with significant edge plane exposure. However, differences in surface exposure of the aforementioned Fe species could explain the differences in activity if Fe is part of an active site. XPS could not be used for surface analysis because the Fe phases were undetectable. Furthermore, if any of the species are exposed, then the HF acid wash should have removed them. The only other alternative explanation is that an active Fe phase is stabilized on the surface and is so scarce that it could not be detected by Mössbauer spectroscopy.

Schulenburg et al. reported very drastic Fe phase changes in the Mössbauer spectra of heat-treated Fe porphyrins after

exposure to sulfuric acid.[18] The researchers reported that the carbide and metallic phases present in the unwashed sample completely disappear and oxidized iron remains along with two additional species with small isomer shifts (0.12 and 0.46 mm/s) and very high quadrupolar splittings (2.75 and 2.93 mm/s, respectively). It was assumed that these species formed from the dissolution of iron into the acid and subsequent adsorption onto sites coordinated by nitrogen groups. The new species were assigned to surface Fe ions that are 4-fold and 6-fold coordinated, and ORR activity was attributed to the 6-fold-coordinated Fe^{3+} species. Such species were not present in any of our HF or HCl washed catalysts or were present in amounts below detection capability. Schulenberg et al. reported an Fe content of 0.47 mol % after the acid wash, of which 18.7 and 30.6% were the above-mentioned species, respectively. On the basis of the TPO/TGA results, the HF-washed CN_x-Fe/Al_2O_3 contained at most 0.5 mol % Fe. Thus, the new species should have been detected if they were present in the same amount. The activity of our materials was in the same activity range as that reported by Schulenberg et al., so our Mössbauer results do not support a hypothesis that the same nitrogen-coordinated active metal sites are present in the highly ORR active CN_x-Fe/Al_2O_3 or CN_x-Fe/SiO_2 samples after being washed with an acid. Both of the washed samples showed slightly different parameters for the oxidized Fe phase and the unwashed samples; however, the new parameters are not close to the values reported for nitrogen-stabilized metal centers.[18] Finally, it should be reported that all attempts to fit the spectra with additional signals with isomer shifts and quadrupolar splittings similar to those of such metal centers have failed.

Conclusions

Characterization by XRD, TEM, and Mössbauer spectroscopy of the Fe phase in active ORR catalysts prepared from acetonitrile pyrolysis over supported metal particles yielded results that are consistent with Fe particles that have catalyzed the formation of carbon fibers. The main species present were metallic γ-Fe, cementite, and oxidized Fe. γ-Fe is observed only because it is encased in the carbon fiber, which inhibits the phase transition to α-Fe by inhibiting the cell volume expansion related to the transition. The oxidized species likely formed from exposure of the other phases to the atmosphere, and oxidation to Fe^{3+} likely occurs through an Fe^{2+} intermediate. Washing the pyrolysis product with concentrated HF removed more of the carbide and oxidized phases, leaving behind more of the metallic Fe. The metal particles could survive the wash because they were encased in carbon. There was no apparent correlation between the activity and any of the Fe phases present. Additionally, there was no strong evidence for the formation of nitrogen-coordinated Fe centers upon exposure of samples to an acid, although some oxidized species still remain. These findings, combined with our earlier results that showed significant ORR activity on Fe-free CN_x catalysts, lead us to suggest that the role of iron in these materials is to catalyze the formation of carbon nanostructures with increased edge plane exposure and possibly with an increased number of nitrogen functional groups on the surface.

Acknowledgment. We gratefully acknowledge the financial support provided for this work by the National Science Foundation through grants NSF-CTS-0437451, NSF-DGE-0221678, and NSF-DMR-0114098 and by the Ohio Department of Development through the Wright Center of Innovation Program.

References and Notes

(1) Matter, P. H.; Biddinger, E. J.; Ozkan, U. S. Non-Precious Metal Oxygen Reduction Catalysts for PEM Fuel Cells. In *Catalysis*; Spivey, J. J., Ed.; The Royal Society of Chemistry: Cambridge, U.K., 2006; Vol. 20; submitted for publication.

(2) van Veen, J. A. R.; van Baar, J. F.; Kroese, K. J. *Chem. Soc., Faraday Trans. 1* **1981**, *77*, 2827.

(3) van Veen, J. A. R.; Visser, C. *Electrochim. Acta* **1979**, *24*, 921.

(4) Jahnke, H.; Schonborn, M.; Zimmerman, G. *Fortschr. Chem. Forsch.* **1976**, *61*, 133.

(5) Bouwkamp-Wijnoltz, A. L.; Visscher, W.; van Veen, J. A. R.; Boellaard, E.; van der Kraan, A. M.; Tang, S. C. *J. Phys. Chem. B* **2002**, *106*, 12993.

(6) Bae, I. T.; Tryk, D. A.; Scherson, D. A. *J. Phys. Chem. B* **1998**, *102*, 4114.

(7) Sun, G. Q.; Wang, J. T.; Gupta, S.; Savinell, R. *J. Appl. Electrochem.* **2001**, *31*, 1025.

(8) Gojkovic, S. L.; Gupta, S.; Savinell, R. F. *J. Electrochem. Soc.* **1998**, *145*, 3493.

(9) Ladouceur, M.; Lalande, G.; Guay, D.; Dodelet, J. P.; Dignard-Bailey, L.; Trudeau, M. L.; Schulz, R. *J. Electrochem. Soc.* **1993**, *140*, 1974.

(10) Lalande, G.; Tamizhmani, G.; Cote, R.; Dignard-Bailey, L.; Trudeau, M. L.; Schulz, R.; Guay, D.; Dodelet, J. P. *J. Electrochem. Soc.* **1995**, *142*, 1162.

(11) Martin Alves, M. C.; Dodelet, J. P.; Guay, D.; Ladouceur, M.; Tourillion, G. *J. Phys. Chem.* **1992**, *96*, 10898.

(12) Gouerec, P.; Biloul, A.; Contamin, O.; Scarbeck, G.; Savy, M.; Barbe, J. M.; Guilard, R. *J. Electroanal. Chem.* **1995**, *398*, 67.

(13) Bron, M.; Fletcher, S.; Hilgendorff, M.; Bogdanoff, P. *J. Appl. Electrochem.* **2002**, *32*, 211.

(14) Matter, P. H.; Zhang, L.; Ozkan, U. S. *J. Catal.* **2006**, *239*, 83.

(15) Lalande, G.; Cote, R.; Guay, D.; Dodelet, J. P.; Weng, L. T.; Bertrand, P. *Electrochim. Acta* **1997**, *42*, 1379.

(16) Lefevre, M.; Dodelet, J. P.; Bertrand, P. *J. Phys. Chem. B* **2002**, *106*, 8705.

(17) Lefevre, M.; Dodelet, J. P.; Bertrand, P. *J. Phys. Chem. B* **2005**, *109*, 16718.

(18) Schulenburg, H.; Stankov, S.; Schuenemann, V.; Radnik, J.; Dorbandt, I.; Fiechter, S.; Bogdanoff, P.; Tributsch, H. *J. Phys. Chem. B* **2003**, *107*, 9034.

(19) Jain, M.; Chou, S.-h.; Siedle, A. *J. Phys. Chem. B* **2006**, *110*, 4179.

(20) Gojkovic, S.; Gupta, S.; Savinell, R. *J. Electroanal. Chem.* **1999**, *462*, 63.

(21) Gouerec, P.; Biloul, A.; Contamin, O.; Scarbeck, G.; Savy, M.; Riga, J.; Weng, L. T.; Bertrand, P. *J. Electroanal. Chem.* **1997**, *422*, 61.

(22) Wiesener, K. *Electrochim. Acta* **1986**, *31*, 1073.

(23) Matter, P. H.; Wang, E.; Arias, M.; Biddinger, E. J.; Ozkan, U. S. *J. Phys. Chem. B* **2006**, *110*, 18374.

(24) Matter, P. H.; Ozkan, U. S. *Catal. Lett.* **2006**, *109*, 115.

(25) Strelko, V. V.; Kartel, N. T.; Dukhno, I. N.; Kuts, V. S.; Clarkson, R. B.; Odintsov, B. M. *Surf. Sci.* **2004**, *548*, 281.

(26) Strelko, V. V.; Kuts, V. S.; Thrower, P. A. *Carbon* **2000**, *38*, 1499.

(27) Khomenko, V. G.; Barsukov, V. Z.; Katashinskii, A. S. *Electrochim. Acta* **2005**, *50*, 1675.

(28) Matter, P. H.; Wang, E.; Ozkan, U. S. *J. Catal.* **2006**, *243*,395.

(29) Matter, P. H.; Wang, E.; Arias, M.; Biddinger, E. J.; Ozkan, U. S. *J. Mol. Catal.* in press, 2006.

(30) Kinoshita, K. *Carbon, Electrochemical, and Physiochemical Properties*; Wiley-Interscience: New York, 1988.

(31) Chen, P.; Fryling, M. A.; McCreery, R. L. *Anal. Chem.* **1995**, *67*, 3115.

(32) Cline, K. K.; McDermott, M. T.; McCreery, R. L. *J. Phys. Chem.* **1994**, *98*, 5314.

(33) Faubert, G.; Cote, R.; Guay, D.; Dodlet, J. P.; Denes, G.; Bertrand, P. *Electrochim. Acta* **1998**, *43*, 341.

(34) Fournier, J.; Lalande, G.; Cote, R.; Guay, D.; Dodlet, J. P. *J. Electrochem. Soc.* **1997**, *144*, 218.

(35) Bard, A. J.; Faulkner, L. R. *Electrochemical Methods: Fundamentals and Applications*; John Wiley and Sons: New York, 2001.

(36) Faubert, G.; Cote, R.; Guay, D.; Dodelet, J. P.; Denes, G.; Poleunis, C.; Bertrand, P. *Electrochim. Acta* **1998**, *43*, 1969.

(37) Audier, M.; Bowen, P.; Jones, W. *J. Cryst. Growth* **1983**, *64*, 291.

(38) Herreyre, S.; Gadelle, P.; Moral, P.; Millet, J. M. M. *J. Phys. Chem Solids* **1997**, *58*, 1539.

(39) Le Caer, G.; Dubois, J. M.; Senateur, J. P. *J. Solid State Chem.* **1976**, *19*, 19.

(40) Bodker, F.; Morup, S.; Linderoth, S. *Phys. Rev. Lett.* **1994**, *72*, 282.

(41) Baker, R. T. K.; Chludzinski, J. J., Jr.; Lund, C. R. F. *Carbon* **1987**, *25*, 295.

(42) Audier, M.; Coulon, M. *Carbon* **1985**, *23*, 317.

(43) Borsa, D. M.; Boerma, D. O. *Hyperfine Interact.* **2003**, *151/152*, 31.
(44) Borowski, M.; Traverse, A.; Eymery, J.-P. *Nucl. Instr. Methods Phys. Res. B* **1997**, *122*, 247.
(45) Cabral, F. A. O.; Araujo, J. H. d.; Araujo, R. C.; Gama, S. *J. Appl. Phys.* **1998**, *83*, 6932.
(46) Cai, Y.; Li, A.; Cao, J.; Ni, X.; Zhang, G.; Yu, G.; Xu, W. *Nucl. Instrm. Methods Phys. Res., Sect. B* **2000**, *168*, 422.
(47) Dubey, R.; Guptaa, A. *J. Appl. Phys.* **2005**, *98*.
(48) Schaaf, P.; Lieb, K.-P.; Carpene, E.; Han, M.; Landry, F. *Czech. J. Phys.* **2001**, *51*.
(49) Gibb, T. C. *Principles of Mössbauer Spectroscopy*; Chapman and Hall: London, 1976.
(50) Bussiere, P. Mössbauer Spectroscopy - Nuclear Gamma Resonance. In *Catalyst Characterization: Physical Techniques for Solid Materials*; Vedrine, J. C., Ed.; Plenum Publishing Corporation: New York, 1994.